BIOMASS AND BIOENERGY 35 (2011) 3481–3495

Available at www.sciencedirect.com

ScienceDirect

http://www.elsevier.com/locate/biombioe

Mathematical modelling of a continuous biomass torrefaction reactor: TORSPYD™ column

J. Ratte[*], *E. Fardet*, *D. Mateos*, *J.-S. Héry*

Thermya, 1 rue Nicolas Appert, 33140 Villenave D'ornon, France

ARTICLE INFO

Article history:
Received 20 July 2010
Received in revised form
18 April 2011
Accepted 22 April 2011
Available online 31 May 2011

Keywords:
Modelling
Torrefaction
Wood
Biomass
Depolymerisation
Co-Combustion

ABSTRACT

Torrefaction is a soft thermal process usually applied to cocoa or coffee beans to obtain the Maillard reaction to produce aromatics and enhance the flavour. In the case of biomass the main interest of torrefaction it is to break the fibers. To do so, Thermya company has developed and patented a biomass torrefaction/depolymerisation process called TORSPYD™. It is a homogeneous "soft" thermal process that takes place in an inert atmosphere. The process progressively eliminates the biomass water content transforms a portion of the biomass organic matter and breaks the biomass structure by depolymerisation of the fibers. This produces a high performance solid fuel, called Biocoal, which offers a range of benefits over and above that of normal biomass fuel. To develop such a process, this company has developed two main tools:

- a continuous torrefaction laboratory pilot with a capacity to produce 3 – 8 kg/h of torrefied biomass;
- a mathematical model dedicated to the design and optimisation of the TORSPYD reactor.

The mathematical model is able to describe the chemical and physical processes that take place in the torrefaction column at two different scales, namely: the particle, and the surrounding gas. The model enables the gas temperature profiles inside the column to be predicted, and the results of the model are then validated through experiment in the laboratory pilot. The model also allows us to estimate the thermal power necessary to torrefy any type of biomass for a given moisture content.

© 2011 Elsevier Ltd. All rights reserved.

1. Introduction

Biomass has been used as a source of energy ever since man started burning wood to cook or keep warm; nowadays, biomass is still the world's second largest source of renewable energy. Thermya is an engineering company dedicated to biomass conversion for the production of carbon and solid fuels. It has developed and finalized a process for the production of a high energy yield fuel out of non-food biomass; this biocoal product is stable, easily grindable, dry and non-hygroscopic. This process can eliminate the limitations on the combustion of raw biomass (pellets or chips) in industrial boilers.

Raw biomass has a high water content, which varies according to its nature; wood, for example, contains 45%–60% of water. This presence of water generates many constraints in the biomass valorisation chain and affects its profitability. The important physical volume and very low density of raw biomass restrict the productivity of its collection. Due to its physico-chemical nature, raw biomass requires high-pressure

---

[*] *Corresponding author*. Tel.: +33 556 151 364; fax: +33 556 451 997.
E-mail address: ratte@thermya.com (J. Ratte).

0961-9534/$ – see front matter © 2011 Elsevier Ltd. All rights reserved.
doi:10.1016/j.biombioe.2011.04.045

compacting operations to be transformed into pellets. From an energy point of view, raw biomass performs poorly: its combustion in thermal power station boilers demands costly fittings and on-going maintenance. Furthermore, if co-combustion is performed with biomass and coal, raw biomass requires special infrastructure for storage and for grinding because its high content of fibers requires high energy levels. Table 1 summarizes the grinding energy necessary for different solid fuels.

Biomass torrefaction by depolymerisation consists of a “soft” heat treatment (<250 °C) allowing the definitive elimination of the biomass water as well as a transformation of a part of the biomass organic matter. The biomass is uniformly heated. The torrefaction process dries the biomass, makes it irreversibly non-hygroscopic and concentrates its energy potential into an easily transportable and grindable solid fuel. Grinding torrefied biomass, for instance, requires less than a quarter of the energy required to grind fresh wood (Table 1).

The TORSPYD torrefaction process, allows conversion of all kinds of ligno-cellulosic biomass into BioCoal. BioCoal, which contains less than 1% moisture, retains 95% of the initial biomass energy and has more than 90% of its initial dry mass. BioCoal’s net calorific value is around 20,500 kJ/kg; far greater than that of non-torrefied biomass. As a result of its very low moisture content and non-hygroscopic properties BioCoal cannot undergo any biological degradation and as a result it can be stored and shipped safely without any risk linked to storage conditions. Biomass torrefaction also opens up opportunities for manufacturers of classical wood pellets or forest operators, whose production could gain considerable value from torrefaction. Classical pellets are commonly produced from sawdust or from co-products of the primary wood processing industry, whereas TORSPYD technology is designed to produce premium quality biomass fuel (totally dry and non-hygroscopic) directly from forestry or agriculture residues. In addition, producing premium quality pellets from torrefied wood is less energy-consuming than producing classical wood pellets [2]. Furthermore, torrefied wood pellets have got better properties (moisture content, LHV) than standard wood pellets [3], which makes them a better solid fuel.

Wood is constituted by hemicellulose (20–32 wt% for coniferous wood [4]), cellulose (35–50 wt% for coniferous wood [4]), lignin (20–32 wt% for coniferous wood [4]) and organic and mineral matters (<3%). During the thermal depolymerisation, the molecular structure of the wood is modified which provokes a change in its properties. The progressive heating of the biomass and rather its uniform depolymerisation frees the water held within the biomass, and evaporates volatile organic matters (VOC). The heat decomposites the hemicellulose. At the relatively low temperature at which the TORSPYD process operates (<250 °C) the lignin undergoes a minor modification whereas the cellulose is not attacked in any way by the heat. Fig. 1 represents a thermogravimetric analysis (TGA) of the different wood compounds [5].

Table 1 – Energy requirement for grinding of different solid fuels.

Type of solid	Grinding energy (kWh/t)	Finess	Reference
Beech	850	100% < 500 μm	[1]
Torrefied beech (at 240 °C)	200	100% < 500 μm	[1]
Torrefied pin (at 240 °C)	140	95% < 100–150 μm	Measured by ABAC-CFH for Thermya
Lignite	65	95% < 80–90 μm	Measured by ABAC-CFH

From this TGA analysis [5], one can deduct that hemicellulose is the most reactive compound as it starts to decompose from 220 °C. Up to 250 °C, lignin deteriorates itself gradually. Cellulose only starts degrading above 300 °C. As the hemicellulose plays a fundamental role in the preservation of the parietal organized architecture (by linking the fibers of cellulose to each other) its depolymerisation and its devolatilization weaken the whole structure; as a consequence the wood becomes highly friable. Furthermore, as the hemicellulose is an amorphous polymer with a large capacity to absorb humidity, its degradation allows the elimination of water and the production of a non-hygroscopic wood. Once evaporated the water cannot be reabsorbed by the wood anymore.

In order to produce this specific biomass fuel, our company developed a unique and innovative process for the fast and continuous conversion of raw biomass into a dry, non-hygroscopic, dense and easy-to-grind material ([6] [7],). This new process, called TORSPYD, is based on the SPD principle (“Scaled Pyrolytic Distillation”). The SPD does not require any thermal pre-treatment of the biomass. It only undergoes a primary crushing step (G50 crushing range). Basically, in an SPD column takes place a processus of organic solid distillation. A solid organic particle introduced at the top of the column goes down step by step and loses part of its matter content at each step; it moves down the column very gradually and progressively increases in temperature. In this way, the biomass first loses all its water and then gradually starts to loose organic matter (Fig. 2). The characteristics of the torrefied biomass produced depend on the process conditions, and most particularly the temperature conditions. During its progression through the column, wood undergoes several phenomena: heating, drying and thermal degradation. In order

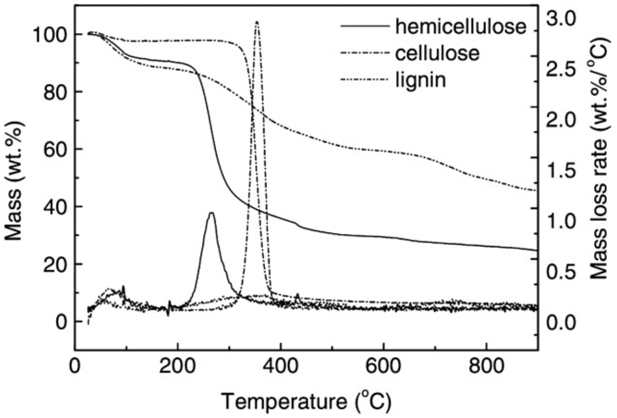

Fig. 1 – TGA analysis of hemicelluloses, cellulose and lignin.

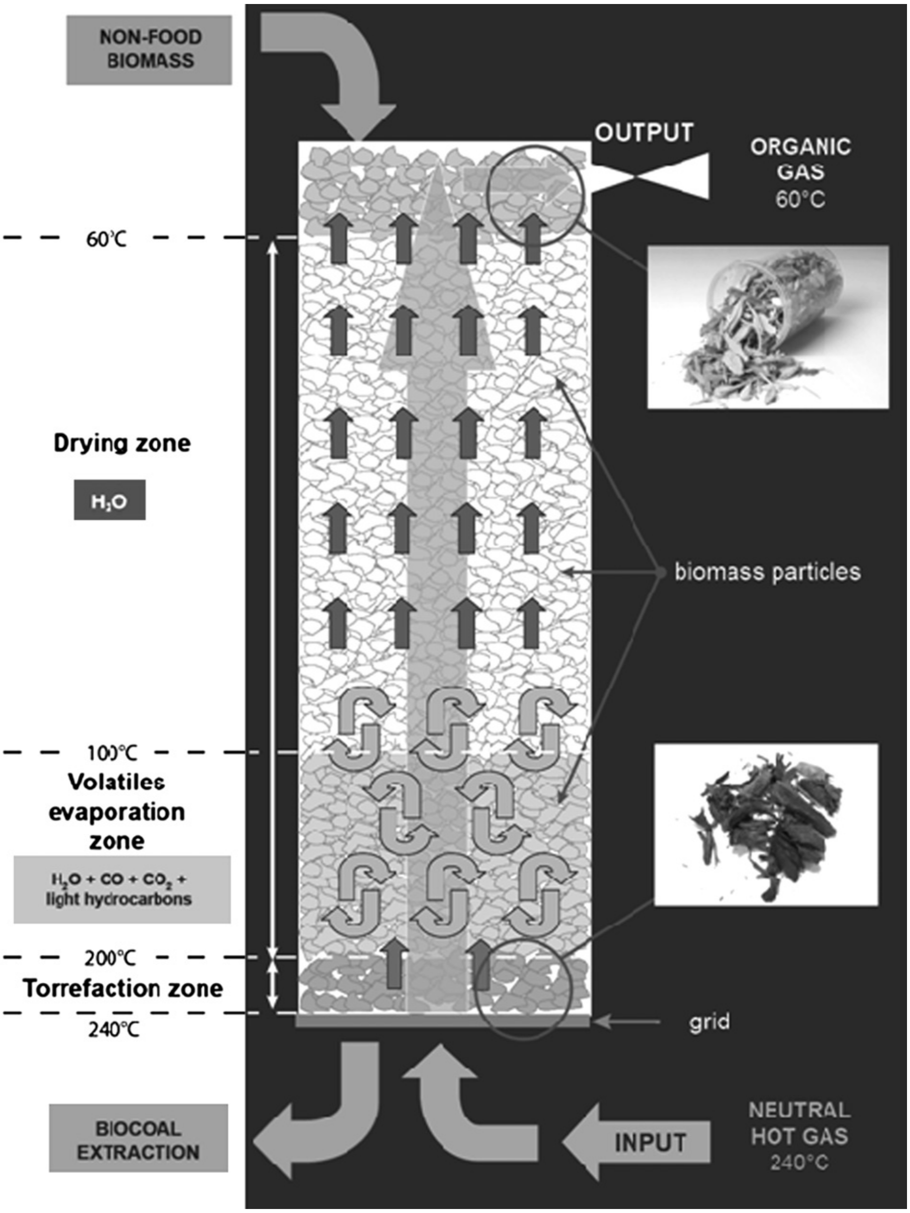

Fig. 2 – DPE description.

to gain a thorough knowledge of these phenomena, a mathematical modelling was created to describe the behaviour of a continuous torrefaction reactor: TORSPYD column.

2. Mathematical modelling of a continuous torrefaction reactor

Previously, the torrefaction thermal degradation has been presented. The scope of this part is to describe a mathematical modelling of the behaviour of the particle and the gas inside the TORPSPYD column. Such a topic has already been studied in the literature. For example, the work of Fonseca Felfli et al. [8] can be cited. In this work, a mathematical model valid for the torrefaction of biomass briquettes is presented. For the heating up of a dried wood piece between 503 and 573 K, it describes physical and chemical processes inside the wood particle. Chemical torrefaction reactions are modelled by the way of the Shafizadeh and Chin [9] model pathway in which wood (W) is thermal degradated in three competitive reactions to gas (G), tar (T) and charcoal (C) (Fig. 3).

$k_i = A_i \exp(-E_i/(R_g T))$ represents the reaction constant rate for the reaction i.

In the present paper, a mathematical model of a torrefaction reactor is established. It is able to plot different profiles inside a particle (compositions, temperature, pressure) at different positions inside the column and at different times. In addition, the evolution of the compositions, the temperature, and the velocity of the convective gas surrounding the particle bed can be represented for different position in the column and also at different times. Firstly, it is important to explain the algorithm that has been developed for accomplishing this task.

$$W_{(s)} \xrightarrow{k_1} G_{(g)} \quad 1$$

$$W_{(s)} \xrightarrow{k_2} T_{(g)} \quad 2$$

$$W_{(s)} \xrightarrow{k_3} C_{(s)} \quad 3$$

Fig. 3 – Shafizadeh and Chin model [7].

2.1. *Problem formulation*

The TORSPYD reactor is decomposed into two sub-systems. The complexity of modelling this kind of reactor arises from the fact that the column is a double porous media (Fig. 4).

The system particles/gas forms by itself a first porous media and its porosity is a function of particle size. In addition, at a smaller scale, a wood particle is a heterogeneous material that can be composed of fives phases: dried wood phase, char phase, bound water phase, liquid water phase and gas phase (a multi-component phase).

The TORSPYD column is formed by packed particles of wood undergoing torrefaction thermal degradation and a convective gas surrounding the particle bed: these two sub-systems exchange heat and gas (Fig. 5).

From the work of Ratte et al. [10], a mathematical model has been created that includes the drying and the transport of the particles, the thermal degradation of wood in the column and the evolution of different characteristics of the convective gas (temperature, composition, velocity). But before writing this model, it is necessary to describe in more details the phenomena that occur in the column.

2.2. *Drying and thermal degradation reactions*

During thermal degradation of organic matter, there is a mix between mass transfer, energy transfer and chemical reactions that are responsible of the conversion of wood material. But before those reactions take place inside wood particles, the temperature of the biomass must be at least 200 °C.

During the heating up of the material, thermal degradation is always proceeded by a drying step. Indeed, wood contains initially water in different forms (free or liquid water, bound water and water vapour). Evaporation of both liquid and bound water is required to permit the material to reach a temperature at which thermal degradation reactions can be promoted. This drying step should not be neglected in term of process time and in term of energy cost.

For modelling the drying step, all the details can be found in Ratte et al. [10] from the works of Whitaker [11] about drying.

Concerning the thermal degradation, as it was seen before, torrefaction reactions produce gas, tar and char. The Shafizadeh and Chin [9] model has already been used to model torrefaction of wood briquettes [8]. Recently, Casajus

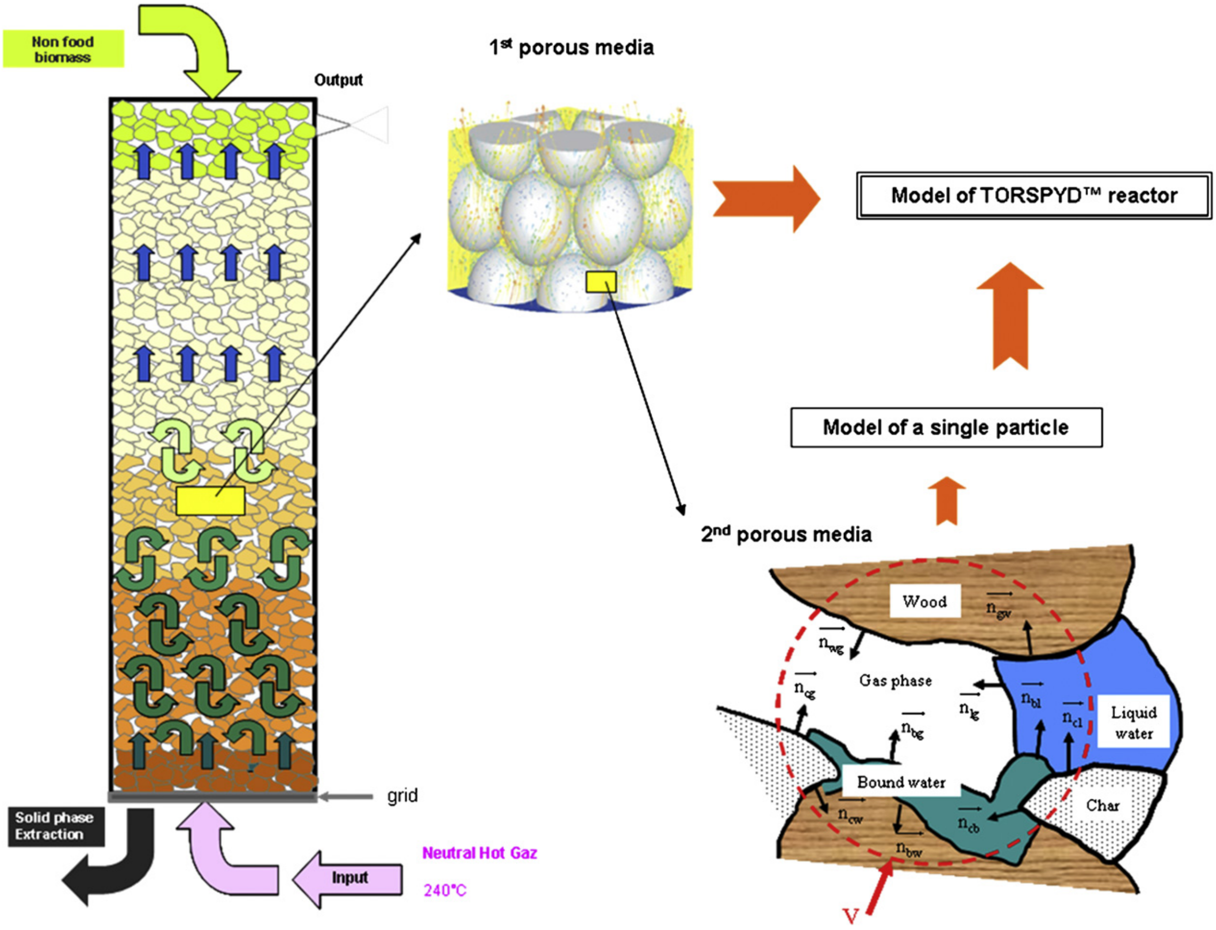

Fig. 4 – TORSPYD™ column: a double porous media.

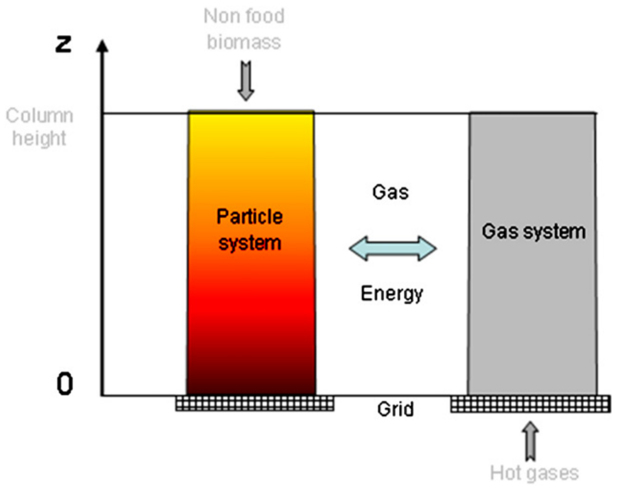

Fig. 5 – Formulation of the problem.

[12] has validated that the Shafizadeh and Chin [9] model is well adapted to represent torrefaction for wood.

Regarding this chemical model pathway for torrefaction process, kinetic parameters (Table 2) can be found in the literature [13].

Consequently, the Shafizadeh and Chin [9] model coupled with Thurner and Mann [13] parameters has been selected to represent heterogeneous reactions. Regarding the knowledge of homogeneous reactions that will be taken in account in the model, a list of several gaseous species has to be established. This list contains nitrogen, water vapour and oxygen because this last component is initially present inside the wood particles. The torrefaction process produces light gases H_2, CH_4, CO, CO_2 [14]. For the production of tars, from TGA-FTIR analysis, Reppelin [14] observed a production of water, formic acid and acetic acid during slow pyrolysis of wood. A list of eleven gaseous species has been detailed in Table 3 including benzene and phenol.

From this list, eight homogeneous reactions have been selected:

- Oxidation

$$-R1:\ CH_4 + O_2 \xrightarrow{k_1^{gas}} CO + 2H_2$$

$$-R2:\ H_2 + 1/_2 O_2 \xrightarrow{k_2^{gas}} H_2O$$

$$-R3:\ CO + 1/_2 O_2 \xrightarrow{k_2^{gas}} CO_2$$

- Water gas shift

$$-R4:\ CO + H_2O \xrightarrow{k_4^{gas}} CO_2 + H_2$$

Table 2 – Kinetic parameters for primary reactions.

Reaction	A [s^{-1}]	E_a [kJ/mol]	Reference
1	14,350	88.6	*Measured by Thurner and Mann [13]*
2	4,125,000	112.7	*Measured by Thurner and Mann [13]*
3	737,700	106.5	*Measured by Thurner and Mann [13]*

Table 3 – Considered gaseous species in the mathematical model.

Product	Formula
Nitrogen	N_2
Oxygen	O_2
Water	H_2O
Hydrogen	H_2
Methane	CH_4
Carbon dioxide	CO
Carbon Oxide	CO_2
Formic acid	$HCOOH$
Acetic acid	CH_3COOH
Phenol	C_6H_5OH
Benzene	C_6H_6

$$-R5:\ CO_2 + H_2 \xrightarrow{k_5^{gas}} CO + H_2O$$

- Acid thermal degradation

$$-R6:\ HCOOH \xrightarrow{k_6^{gas}} CO + H_2O$$

$$-R7:\ HCOOH \xrightarrow{k_7^{gas}} CO_2 + H_2$$

$$-R8:\ CH_3COOH \xrightarrow{k_8^{gas}} CH_4 + CO_2$$

Tars produced during torrefaction process of wood undergo several steps including: condensation, evaporation, thermal cracking and condensation in the column. The condensation and evaporation steps are not considered in the model. After being produced and transferred through particle surfaces to the surrounding gas, tars will encounter colder surfaces (particles, reactor walls). If the surrounding gas at a given temperature is saturated in each tar species, condensation can occur. Except water component, liquid phases for tar species are not modelled to simplify the model. However, thermal cracking of condensable gases is modelled through the eight previous homogeneous reactions. Reaction rate for each reaction is given in Table 4 where concentrations are expressed in mol m^{-3} and reaction rates in mol m^{-3} s^{-1}.

2.3. *Modelling of the particle system*

In order to simplify the problem, some assumptions have to be postulated:

(A0) Inlet wood particles are considered to be spherical and to have a constant radius R_{part};
(A1) Particle transport from the top to the bottom of the reactor is assumed to be a plug flow type;
(A2) Wood particles are neither submitted to agglomeration nor to attrition inside the column.

As it was seen previously, solid particles are extracted by the way of the grid at the bottom of the reactor. Basically, the velocity of the particle U_{part} is not constant but it is a time function U_{part} (t): it is a periodic function. The period T, the instantaneous extraction velocity $U_{extract}$ and the time of extraction $t_{extract}$ are input parameters of this periodic function.

Table 4 – Expression of reaction rate.

Reaction	Reaction rate [mol m^{-3} s^{-1}]	Reference
R1	$r_1 = 100k_1^{gaz}[CH_4]^{0,7}[O_2]^{0,8}$, $k_1^{gaz} = 1.58{*}10^{10}\exp\left(\frac{-202641}{RT}\right)$	*Dryer and Glassman* [15]
R2	$r_2 = 0.001k_2^{gaz}[H_2][O_2]$, $k_2^{gaz} = 1.08{*}10^{10}\exp\left(\frac{-125525}{RT}\right)$	*Kerinin and Shifrin* [16]
R3	$r_3 = k_3^{gaz}[CO][H_2O]^{0,5}[O_2]^{0,25}$, $k_3^{gaz} = 1.78{*}10^{10}\exp\left(\frac{-180032}{RT}\right)$	*Dryer and Glassman* [15]
R4	$r_4 = 0.1k_4^{gaz}[CO][H_2O]$, $k_4^{gaz} = 2.778\exp\left(\frac{-12560}{RT}\right)$	*Biba et al.* [17]
R5	$r_5 = 0.1k_5^{gaz}[CO_2][H_2]$, $k_5^{gaz} = k_4^{gaz}/0.022\exp\left(\frac{3.473 * 10^4}{RT}\right)$	*Biba et al.* [17]
R6	$r_6 = k_6^{gaz}[HCOOH]$, $k_6^{gaz} = 7.49 * 10^{14}\exp\left(\frac{-287483}{RT}\right)$	*Chang et al.* [18]
R7	$r_7 = k_7^{gaz}[HCOOH]$, $k_7^{gaz} = 4.46 * 10^{13}\exp\left(\frac{-286000}{T}\right)$	*Chang et al.* [18]
R8	$r_8 = k_8^{gaz}[CH_3COOH]$, $k_8^{gaz} = 1.32 * 10^{11}\exp\left(\frac{-244000}{T}\right)$	*Blake et al.* [19]

The velocity has to be mathematically computed as a discrete time dynamic model. To overcome it, the grid periodic signal is decomposed into a sum of cosine and sine functions, by the way of a Fourier series expansion:

$$U_{\mathrm{part}}(t) = \frac{a_0}{2} + \sum_{n=1}^{\infty}\left[a_n\cos\left(\frac{2n\pi t}{T}\right) + b_n\sin\left(\frac{2n\pi t}{T}\right)\right], \tag{1}$$

where

$$a_0 = \frac{2}{T}\int_{-T/2}^{T/2} U_{part}(t)dt, \tag{2}$$

$$a_n = \frac{2}{T}\int_{-T/2}^{T/2} U_{part}(t)\cos\left(\frac{2n\pi t}{T}\right)dt, \tag{3}$$

$$b_n = \frac{2}{T}\int_{-T/2}^{T/2} U_{part}(t)\sin\left(\frac{2n\pi t}{T}\right)dt, \tag{4}$$

From the different input parameters described previously, it is possible to express:

$$a_0 = \frac{2 * U_{extract} * t_{extract}}{T}, \tag{5}$$

$$a_n = \frac{U_{extract}}{n\pi}\left[\sin\left(\frac{n\pi}{T}(-T + t_{extrac})\right) - \sin\left(\frac{n\pi}{T}(T - t_{extrac})\right)\right], \tag{6}$$

$$b_n = -\frac{U_{extract}}{n\pi}\left[\cos\left(\frac{n\pi}{T}(T + t_{extract})\right) - \cos\left(\frac{n\pi}{T}(T - t_{extract})\right)\right], \tag{7}$$

U_{part} (t) can be now easily expressed and will be calculated at each time integration step.

Another operating condition is the bed porosity $\epsilon_{\mathrm{react}}$ which is assumed to be constant (assumption A_0). The bed porosity is a conditioner of the number of particles per reactor volume unit n_{part}

$$n_{part} = \frac{1 - \epsilon_{react}}{V_{part}}, \tag{8}$$

n_{part} represents the volume of one particle.

Based on the work of Ratte et al. [10], Table 5 sums up all differential partial and algebraic equations governing evolution of wood spherical particles undergoing TORPSYD.

At the top of the column, wood and char concentrations inside the particles are inputs of the problem. Intra-particular gas composition is conditioned to be water saturated air at inlet temperature. Moisture content (dry basis) M_0 of fresh inlet particles permits to calculate the water concentration of particles. As the temperature is fixed as input parameters, particle energy *H* can be estimated.

This set of Dirichlet type conditions is summarized as following:

$$\textit{for } z = H_{reac} \textit{ and } \forall t, \forall r \quad \langle\rho_w\rangle|_{t,r,z=H_{reac}} = 500\mathrm{kg/m^3}$$

$$\textit{for } z = H_{reac} \textit{ and } \forall t, \forall r \quad \langle\rho_c\rangle|_{t,r,z=H_{reac}} = 0kg/m^3$$

$$\textit{for } z = H_{reac} \textit{ and } \forall t, \forall r \quad M|_{t,r,z=H_{reac}} = M_0$$

$$\textit{for } z = H_{reac} \textit{ and } \forall t, \forall r \quad \langle\rho_i\rangle|_{t,r,z=H_{reac}} = \text{saturated air}$$

$$\textit{for } z = H_{reac} \textit{ and } \forall t, \forall r \quad H|_{t,r,z=H_{reac}} = H$$

Considering gas–solid interfaces, estimating mass and heat flux between the particles and the surrounding gas requires the knowledge of the different mass transfer coefficients $h_{m(i)}$ and the heat transfer coefficient h_T. As the residence time of the particles is much higher than the gas one, the solid bed can be considered as a fixed bed. Therefore mass and heat transfer coefficient will be estimated by using the correlation of Stewart [20].

For each gaseous species i, Sherwood number is calculated for a block of fixed particles [20]:

$$Sh_i = Sc_i^{1/3}Re\left(2.19Re^{-2/3} + 0.78Re^{-0.381}\right), \tag{9}$$

For a fixed bed, Reynolds number is determined by:

$$Re = \frac{2R_{part}\rho_{gas}U_{gas}}{(1 - \epsilon_{reac})\mu_{gas}}, \tag{10}$$

Sherwood number is defined by:

$$Sh_i = \frac{2h_m(i)R_{part}}{D_i(1 - \epsilon_{reac})}, \tag{11}$$

Table 5 – Algebraic and differential equations for the particle system.

Variable	Equation
Wood concentration: $\langle\rho_w\rangle$	Mass Conservation: for $z\#H_{reac}$ and $\forall t,\forall r\ \frac{\partial\langle\rho_w\rangle}{\partial t}=U_{part}(t)\frac{\partial\langle\rho_w\rangle}{\partial z}-(\langle k_1\rangle+\langle k_2\rangle+\langle k_3\rangle)\langle\rho_w\rangle$ for $z=H_{reac}$ and $\forall t,\forall r\ \langle\rho_w\rangle=\langle\rho_w\rangle\vert_{t,r,z=H_{reac}}$
Char concentration: $\langle\rho_c\rangle$	Mass Conservation: for $z\#H_{reac}$ and $\forall t,\forall r\ \frac{\partial\langle\rho_c\rangle}{\partial t}=U_{part}(t)\frac{\partial\langle\rho_c\rangle}{\partial z}+\langle k_3\rangle\langle\rho_w\rangle$ for $z=H_{reac}$ and $\forall t,\forall r\ \langle\rho_c\rangle=\langle\rho_c\rangle\vert_{t,r,z=H_{reac}}$
Total water concentration: $\langle\rho_l\rangle+\langle\rho_b\rangle+\langle\rho_{H_2O(g)}\rangle$	Mass Conservation: for $z\#H_{reac}$, for $r=0$ and $\forall t\ \left.\frac{\partial(\langle\rho_l\rangle+\langle\rho_b\rangle+\langle\rho_{H_2O(g)}\rangle)}{\partial r}\right\vert_{t,0}=0$ for $z\#H_{reac}$, for $r\#0$, $r\#R_{part}$ and $\forall t\ \frac{\partial(\langle\rho_l\rangle+\langle\rho_b\rangle+\langle\rho_{H_2O(g)}\rangle)}{\partial t}-U_{part}(t)\frac{\partial(\langle\rho_l\rangle+\langle\rho_b\rangle+\langle\rho_{H_2O(g)}\rangle)}{\partial z}+\nabla\cdot(\langle\rho_l\rangle^l\langle\mathbf{v}_l\rangle)+\nabla\cdot(\langle\rho_b\mathbf{v}_b\rangle)+\nabla\cdot(\langle\rho_{H_2O(g)}\rangle^g\langle\mathbf{v}_g\rangle)$ $-\nabla\cdot\left\{\left\langle\rho_g\right\rangle^g\left[\epsilon_g D_{eff}^{H_2O(g)}\cdot\nabla\left(\frac{\left\langle\rho_{H_2O(g)}\right\rangle^g}{\left\langle\rho_g\right\rangle^g}\right)\right]\right\}=\left\langle R_{H_2O(g)}^{hetrogeneous}\right\rangle+\left\langle R_{H_2O(g)}^{homogeneous}\right\rangle$ for $z\#H_{reac}$, for $r=R_{part}$ and $\forall t\ \frac{\partial(\langle\rho_l\rangle+\langle\rho_b\rangle+\langle\rho_{H_2O(g)}\rangle)}{\partial t}-U_{part}(t)\frac{\partial(\langle\rho_l\rangle+\langle\rho_b\rangle+\langle\rho_{H_2O(g)}\rangle)}{\partial z}+\nabla\cdot(\langle\rho_l\rangle^l\langle\mathbf{v}_l\rangle)+\nabla\cdot(\langle\rho_b\mathbf{v}_b\rangle)+\nabla\cdot(\langle\rho_{H_2O(g)}\rangle^g\langle\mathbf{v}_g\rangle)$ $-\nabla\cdot\left\{\left\langle\rho_g\right\rangle^g\left[\epsilon_g D_{eff}^{H_2O(g)}\cdot\nabla\left(\frac{\left\langle\rho_{H_2O(g)}\right\rangle^g}{\left\langle\rho_g\right\rangle^g}\right)\right]\right\}=\left\langle R_{H_2O(g)}^{heterogeneous}\right\rangle+\left\langle R_{H_2O(g)}^{homogeneous}\right\rangle\Bigg(\langle\rho_l\rangle^l\langle\mathbf{v}_l\rangle+\langle\rho_b\mathbf{v}_b\rangle+\left\langle\rho_{H_2O(g)}\right\rangle^g\langle\mathbf{v}_g\rangle$ $-\left\langle\rho_g\right\rangle^g D_{eff}^{H_2O(g)}\cdot\nabla\left(\frac{\left\langle\rho_{H_2O(g)}\right\rangle}{\left\langle\rho_g\right\rangle}\right)\Bigg)\cdot\mathbf{n}=h_{m(H_2O(g))}\left(\left\langle\rho_{H_2O(g)}\right\rangle^g-\rho_{gas(H_2O(g))}\right)$ for $z=H_{reac}$ and $\forall t,\ \forall r\quad M=M\vert_{t,r,z=H_{reac}}$
Water vapour concentration : $\langle\rho_{H_2O(g)}\rangle$	Thermodynamical equilibrium : $\forall r,\forall z$ and $\forall t\quad\langle\rho_{H_2O(g)}\rangle=f(M,\langle T\rangle)$ ([8])
Particle porosity: ϵ_g	$\forall r$ and $\forall t\quad\epsilon_g=1-\left(\frac{\langle\rho_w\rangle}{\langle\rho_w\rangle^w}+\frac{\langle\rho_c\rangle}{\langle\rho_c\rangle^c}+\frac{\langle\rho_l\rangle}{\langle\rho_l\rangle^l}+\frac{\langle\rho_b\rangle}{\langle\rho_b\rangle^b}\right)$
Gaseous species i concentration (except water): $\langle\rho_i\rangle$	Mass Conservation: for $z\#H_{reac}$, for $r=0$ and $\forall t\ \left.\frac{\partial\langle\rho_i\rangle}{\partial r}\right\vert_{t,0}=0$ for $z\#H_{reac}$, for $r\#0, r\#R_{part}$, and $\forall t\ \frac{\partial\langle\rho_i\rangle}{\partial t}-U_{part}(t)\frac{\partial\langle\rho_i\rangle}{\partial z}+\nabla\cdot(\langle\rho_i\rangle^g\langle\mathbf{v}_g\rangle)=\langle R_i^{heterogenous}\rangle+\langle R_i^{homogenous}\rangle+\nabla\cdot\left\{\langle\rho_g\rangle^g\left[\epsilon_g D_{eff}^i\cdot\nabla\left(\frac{\langle\rho_i\rangle^g}{\langle\rho_g\rangle^g}\right)\right]\right\}$ for $z\#H_{reac}$, for $r=R_{part}$, $\forall t$ and for $i\#N_2\ \frac{\partial\langle\rho_i\rangle}{\partial t}-U_{part}(t)\frac{\partial\langle\rho_i\rangle}{\partial z}+\nabla\cdot(\langle\rho_i\rangle^g\langle\mathbf{v}_g\rangle)=\langle R_i^{heterogenous}\rangle+\langle R_i^{homogenous}\rangle+\nabla\cdot\left\{\langle\rho_g\rangle^g\left[\epsilon_g D_{eff}^i\cdot\nabla\left(\frac{\langle\rho_i\rangle^g}{\langle\rho_g\rangle^g}\right)\right]\right\}$ $\left(\langle\rho_i\rangle^g\langle\mathbf{v}_g\rangle-\left\langle\rho_g\right\rangle^g D_{eff}^{i(g)}\cdot\nabla\left(\frac{\left\langle\rho_{i(g)}\right\rangle}{\left\langle\rho_g\right\rangle}\right)\right)\cdot\mathbf{n}=h_{m(i)}\left(\langle\rho_i\rangle^g-\rho_{gaz(i)}\right)$ for $z\#H_{reac}$, for $r=R_{part}$ and $\forall t$ and for $i=N_2\quad\langle\rho_g\rangle^g=\rho_{gaz}$ for $z=H_{reac}$ and $\forall t,\forall r,\forall i\quad\langle\rho_i\rangle=\langle\rho_i\rangle\vert_{t,r,z=H_{reac}}$

Total gas concentration in the gas phase: $\langle\rho_g\rangle^g$	Summation : $\forall r$ and $\forall t \quad \langle\rho_g\rangle^g = \frac{1}{\epsilon_g}\sum_{i}^{NGS}\langle\rho_i\rangle$
Energy: H	Energy conservation: for $z\#H_{reac}$, for $r=0$ and $\forall t \quad \left.\frac{\partial H}{\partial r}\right\|_{t,0} = 0$ for $z\#H_{reac}$, for $r\#0$, $r\#R_{part}$ and $\forall t \quad \frac{\partial H}{\partial t} - U_{part}(t)\frac{\partial H}{\partial z} + \nabla\cdot\langle\rho_l\mathbf{v}_l\rangle\langle h_l\rangle^l + \nabla\cdot\langle\rho_b\mathbf{v}_b\rangle\langle h_b\rangle^b + \sum_i^{nc}\nabla\cdot\langle\rho_i\mathbf{v}_i\rangle\langle h_i\rangle^g = \nabla\cdot(\lambda_{eff}\nabla\langle T\rangle)$ for $z\#H_{reac}$, for $r=R_{part}$ and $\forall t \quad \frac{\partial H}{\partial t} - U_{part}(t)\frac{\partial H}{\partial z} + \nabla\cdot\langle\rho_l\mathbf{v}_l\rangle\langle h_l\rangle^l + \nabla\cdot\langle\rho_b\mathbf{v}_b\rangle\langle h_b\rangle^b + \sum_i^{nc}\nabla\cdot\langle\rho_i\mathbf{v}_i\rangle\langle h_i\rangle^g = \nabla\cdot(\lambda_{eff}\nabla\langle T\rangle)\left(\langle\rho_l\rangle^l\langle\mathbf{v}_l\rangle\langle h_l\rangle^l + \langle\rho_b\mathbf{v}_b\rangle\langle h_b\rangle^b + \sum_i\left(\langle\rho_i\rangle\langle\mathbf{v}_g\rangle^g\right.\right.$ $\left.\left.-\left\langle\rho_g\right\rangle^g D^i_{eff}\cdot\nabla\left(\frac{\langle\rho_i\rangle}{\left\langle\rho_g\right\rangle}\right)\right)\langle h_i\rangle^g - \lambda eff\ \nabla\langle T\rangle\right)\cdot\mathbf{n} = h_T(\langle T\rangle - T_{gaz}) + \sum_i h_{m(i)}\left(\langle\rho_i\rangle^g - \rho_{gaz(i)}\right) * \langle h_i\rangle^g$ for $z=H_{reac}$ and $\forall t$, $\forall r \quad H\|_{t,r,z=H_{reac}} = H$
Temperature: $\langle T\rangle$	$\forall r$ and $\forall t \quad H = \langle\rho_w\rangle\langle h_w\rangle^w + \langle\rho_c\rangle\langle h_c\rangle^c + \langle\rho_l\rangle\langle h_l\rangle^l + \langle\rho_b\rangle\langle h_b\rangle^b + \sum_i^{nc}\langle\rho_i\rangle\langle h_i\rangle^g$ $\langle h_j\rangle^j = h_j^{ref} + \int_{T^{ref}}^{\langle T\rangle} Cp_j dT$ where j = Wood, char, liquid water, bound water, gaseous species j
Gas pressure: $\langle P_g\rangle^g$	for $r\#R$ and $\forall t \quad \langle P_g\rangle^g = \frac{\langle\rho_g\rangle^g R_g\langle T\rangle}{M_g}$

And Schmidt numberSc_i is estimated by:

$$Sc_i = \frac{\mu_{gas}}{\rho_{gas}D_i}, \tag{12}$$

In the previous expression, ρ_{gas} is the surrounding gas density, U_{gas} is the superficial velocity of the gas and μ_{gas} is the dynamic viscosity of the surrounding gas. These two first properties are state variables of the model whereas the dynamic viscosity is calculated by ponderate mass average on the viscosities of each gas species [10], depending on the gas temperature. The calculation of the molecular diffusity D_i of the species i in the gas can be found in Ratte et al. [10].

Nusselt number, which leads to the heat transfer coefficient, is evaluated by:

$$Nu = Pr^{1/3}Re\left(2.19Re^{-2/3} + 0.78Re^{-0.381}\right), \tag{13}$$

where Nusselt number Nu and Prandtl number Pr are estimated by:

$$Nu = \frac{2h_t R_{part}}{\lambda_{gaz}(1-\epsilon_{reac})}, \tag{14}$$

$$Pr = \frac{\mu_{gas}Cp_{gas}}{\lambda_{gas}}, \tag{15}$$

Gas thermal conductivity λ_{gas} and specific heat of the gas Cp_{gas} are also calculated by ponderate mass average [10].

2.4. *Modelling of the gas system*

The gas flow through a particle bed is a tri-dimensional phenomenon, governed by momentum conservation equation. In order to simplify the mathematical model problem of TORPSPYD reactor, it required a set of assumptions:

(A3) Gas transport from the bottom to the top of the column is assumed to be a plug flow type;
(A4) The gas is considered to be a perfect gas because of the closed atmospheric pressure prevailing inside the column;
(A5) Diffusion and conduction are neglected in the gas phase;
(A6) Evolution of gas kinetic energy is neglected;
(A7) Although tars are condensable, condensation of those gaseous species will not be considered in the reactor.

Considering assumption (A7), transport of gaseous species in the reactor in governing by the following equations:

$$\frac{\partial\rho_i^{gas}}{\partial t} = -\frac{\partial\rho_i^{gas}U_{gas}}{\partial z} + h_m(i)\left(\langle\rho_i\rangle_{r=R_{part}} - \rho_i^{gas}\right)n_{part}S_{part} + R_{gas}^{homogeneous}(i), \tag{16}$$

This equation allows to determine the accumulation of the gaseous species i balanced by a term of convection transport due to gas velocity U_{gas}, by matter exchanges with the solid particles and homogeneous chemical reaction production of i$R_{gas}^{homogeneous}(i)$.

Table 6 – Algebraic and differential equations for the gas system.

Variable	Equation
Gaseous species i concentration in the gas: ρ_i^{gas}	Mass conservation : *for* $z\#0, t\#0$ $\frac{\partial \rho_i^{gas}}{\partial t} = -\frac{\partial \rho_i^{gas} U_{gas}}{\partial z} + h_m(i)(\langle \rho_i \rangle_{r=R_{part}} - \rho_i^{gas}) n_{part} S_{part} + R_{gas}^{\mathrm{homogeneous}}(i)$ *for* $z = 0, t\#0$ $\rho_i^{gas} = \rho_i^{gas}\vert_{t,z=0}$
Gas energy: H_{gas}	Energy conservation : *for* $z\#0, t\#0$ $\frac{\partial H_{gas}}{\partial t} = -\frac{\partial \sum_i \rho_i^{gas} h_i^{gas} U_{gas}}{\partial z} + \sum_i h_m(i) \langle h_i \rangle^g_{r=R_{part}} (\langle \rho_i \rangle_{r=R_{part}} - \rho_i^{gas})\, n_{part} S_{part} + h_T(\langle T \rangle - T_{gas})\, n_{part} S_{part} + \frac{4}{D_{reac}^{int}} H_{global}(T_{ext} - T_{gas})$ *for* $z = 0, t\#0$ $H_{gas} = H_{gas}\vert_{t,z=0}$
Gas temperature : T_{gas}	∀z and ∀t $H_{gas} = \sum_i \rho_i^{gas} h_i^{gas}$
Velocity gas: U_{gas}	Total mass conservation : *for* $z\#0, t\#0$ $\frac{\partial \rho_{gas}}{\partial t} = -\frac{\partial \rho_{gas} U_{gas}}{\partial z} + \sum_i h_m(i)(\langle \rho_i \rangle_{r=R_{part}} - \rho_i^{gas}) n_{part} S_{part}$ *for* $z = 0, t\#0$ $U_{gas} = U_{gas}\vert_{t,z=0}$
Total gas concentration: ρ_{gas}	Perfect gas : $\rho_{gas} = \frac{P_{gas} M_{gas}}{R_g T_{gas}}$

Table 7 – State variable of the TORPSPYD reactor.

Variable	Type of equation	Number
$\langle \rho_{BS} \rangle(t,r,z)$	PDE	1
$\langle \rho_c \rangle(t,r,z)$	PDE	1
$(\langle \rho_l \rangle + \langle \rho_b \rangle + \langle \rho_{H_2O(g)} \rangle)(t,r,z)$	PDE	1
$\langle \rho_{H_2O(g)} \rangle(t,r,z)$	Algebraic	1
$\langle \rho_i \rangle(t,r,z)$	PDE	NGS-1
$\langle \rho_g \rangle^g(t,r,z)s$	Algebraic	1
$H(t,r,z)$	PDE	1
$\langle T \rangle(t,r,z)$	Algebraic	1
$\langle P_g \rangle^g(t,r,z)$	Algebraic	1
$\epsilon_g(t,r,z)$	Algebraic	1
Sub total	–	NGS+8
$\rho_i^{gas}(t,z)$	PDE	NGS
$H_{gas}(t,z)$	PDE	1
$T_{gas}(t,z)$	Algebraic	1
U_{gas}	PDE	1
ρ_{gas}	Algebraic	1
Sub total	–	NGS+4
Total	–	*(NGS+8) +(NGS+4)*

In a similar manner, the equation of transport for energy is that of a reactive plug flow subjected to losses of energy at the wall:

$$\frac{\partial \sum_i \rho_i^{gas} h_i^{gas}}{\partial t} = -\frac{\partial \sum_i \rho_i^{gas} h_i^{gas} U_{gas}}{\partial z} + \sum_i h_m(i) \langle h_i \rangle^g_{r=R_{part}} \left(\langle \rho_i \rangle_{r=R_{part}} - \rho_i^{gas} \right) n_{part} S_{part} + h_T(\langle T \rangle - T_{gas}) n_{part} S_{part} + Q_{ext}, \tag{17}$$

Right of the term of accumulation, are represented a term of energy transport of the gaseous species i inside the gas phase, a term of energy exchange due to the transport of material between particles and gas and a term of energy exchange by convection between particles and gas. The last term Qext corresponds to a flux of energy by unit of volume transferred toward the wall by the gas flow through the wall of the reactor. By assuming that this last term is equal to the one transferred from the external surface wall to the environment, Q_{ext} can be expressed:

$$Q_{ext} = \frac{4}{D_{reac}^{int}} H_{global}(T_{ext} - T_{gas}), \tag{18}$$

H_{global}, T_{extand} D_{reac}^{int} respectively represent the global heat exchange coefficient, the external environment temperature and the internal diameter of the column. If this assumption was not established, energy conservation of the metallic wall would have to be solved.

Gas energy conservation can be expressed as following:

$$\frac{\partial H_{gas}}{\partial t} = -\frac{\partial \sum_i \rho_i^{gas} h_i^{gas} U_{gas}}{\partial z} + \sum_i h_m(i) \langle h_i \rangle^g_{r=R_{part}} \left(\langle \rho_i \rangle_{r=R_{part}} - \rho_i^{gas} \right) n_{part} S_{part} + h_T(\langle T \rangle - T_{gas})\, n_{part} S_{part} + \frac{4}{D_{reac}^{int}} H_{global}(T_{ext} - T_{gas}), \tag{19}$$

$$H_{gas} = \sum_i \rho_i^{gas} h_i^{gas}, \tag{20}$$

The summation of the species balance leads to the overall mass conservation:

$$\frac{\partial \rho_{gas}}{\partial t} = -\nabla\cdot\left(\rho_{gas}U_{gas}\right) + \sum_{i} h_m(i)\left(\langle\rho_i\rangle_{r=R_{part}} - \rho_i^{gas}\right) n_{part}S_{part}, \qquad (21)$$

Solving this equation permits to obtain U_{gas} whereas gas density ρ_{gas} is calculated considering the perfect gas:

$$\rho_{gas} = \frac{P_{gas}M_{gas}}{R_g T_{gas}}, \qquad (22)$$

Like the particle system, there is also a set of Dirichlet type conditions for the gas system at the bottom of the column. From a well known gaseous composition at the bottom of the reactor, concentration for each species can be easily established:

$$\text{for } z = 0, t0 \quad \rho_i^{gas}\big|_{t,z=0} = \rho_i^{gas}(t, 0)$$

Gas velocity is estimated as a function of the volumic flowrate and the density of gas, linked the gas composition and the gas temperature:

$$\textit{for } z = 0, t0 \quad U_{gas}\big|_{t,z=0} = \frac{\dot{Q}_{gas}}{S_{reac}\rho_{gas}\big|_{t,z=0}}$$

The gas temperature is fixed to 240 °C which allows calculating the gas energy:

$$\textit{for } z = 0, t0 \quad H_{gas}\big|_{t,z=0} = H_{gas}(240^{\circ}\mathrm{C})$$

The following Table 6 sums up all differential partial and algebraic equations governing evolution of the gas inside the TORPSYD reactor.

2.5. *Modelling TORSPYD reactor*

2.5.1. *Summary of the system*

In order to get an overview of how big the system is to solve, Table 7 sums up all the state variables computed in the model. They are associated with an equation that can be algebraic or differential. The model is composed of (NGS+8)+(NGS+4) equations, where NGS is equal to the total number of gaseous species.

2.5.2. *Numerical method*

The equation model is composed of a set of partial differential equations (time and spatial). First, a spatial discretization step is required to transfer the PDAE system into an ODAE system. The r coordinate only concerns the solid system in which particles will be assumed to be spherical. All partial derivatives depending on r coordinate are discretized using the finite

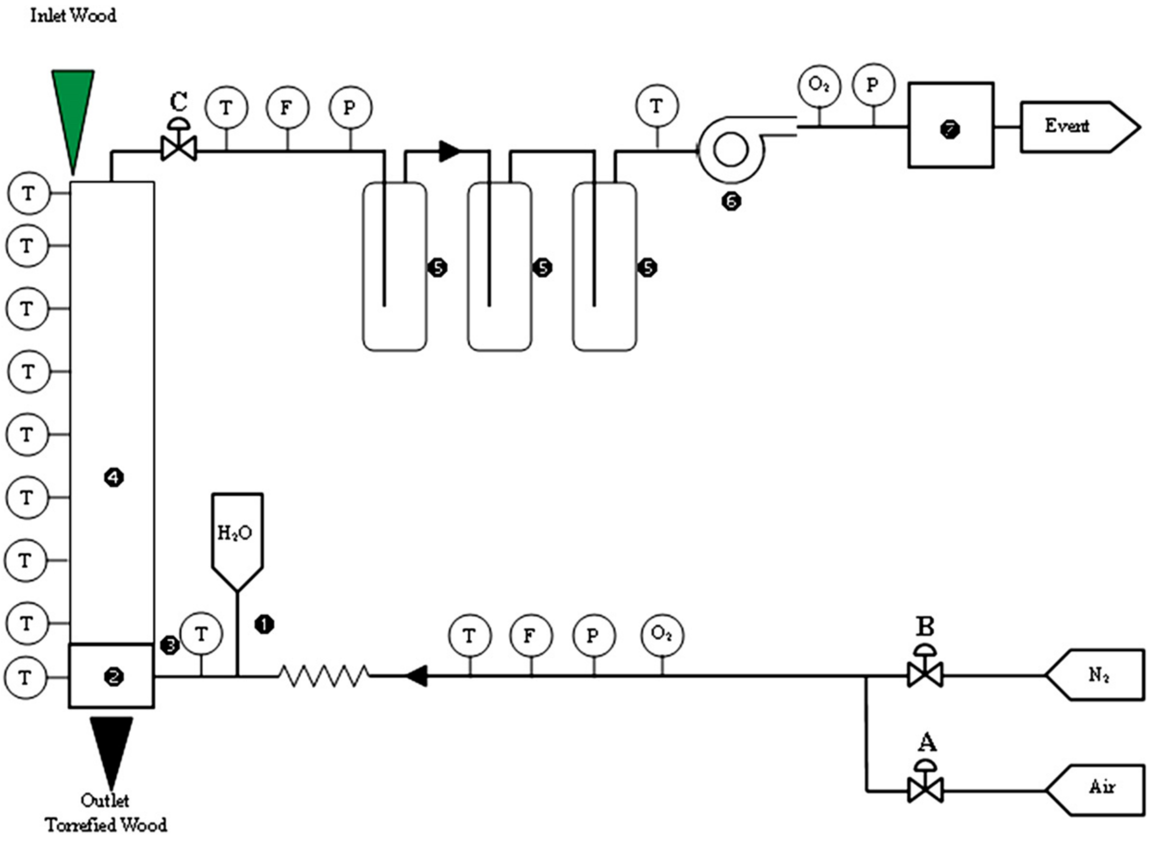

❶: Water injection ; ❷ Injection chamber of hot gas and torrefied wood recovery; ❸ Grid ; ❹ Thermal column containing the biomass beforehand conditioned in terms of size and geometry; ❺ Gas dryer with basic, acid and neutral bath ; ❻ Fan Combustion chamber ; ❼ Gas treatment

A, B, C, D : Valves

Fig. 6 – Process instrument diagram of the continuous pilot reactor.

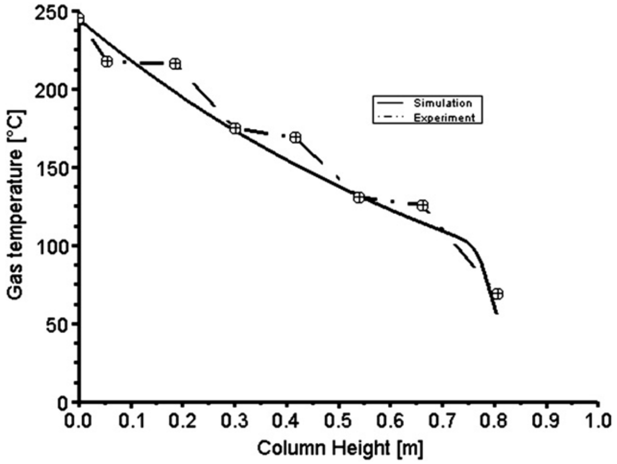

Fig. 7 – Comparison between simulated and experiment results of the gas temperature.

difference method. Concerning partial derivatives depending on z axial coordinate, discretization is performed with finite volume method using an upwind scheme. Control volumes are considered to be non constant in this work. Half of those control volumes are concentrated in the of the height column $H_{reac}/4$. The other half left will describe.

The two methods used consecutively, permit to transfer the system into an ODAE system that can be written in the form of:

$$G(U,t)\frac{dU}{dt} = f(U,t)$$

represents the vector of all state variables of the system.t is the time which will be the integration variable in this work. G is a matrix of which coefficients are functions of U and t.

In order to solve this kind of problem, Gear's method was applied, variable multi-step integration method. The method requires the evaluation of the Jacobian matrix of system. It was evaluated analytically in order to reduce the time resolution of the system.

Simulations were performed on computer (Intel Core2Duo 3.0 GHz 4Go) with Ubuntu 9.10 OS installed.

3. Simulation and experimental validation of TORSPYD reactor

In the model described previously, each state variable depends on time, on r coordinate and/or z coordinate. In this part of the work, many results are presented and the influence of input parameters like the moisture content of the inlet particles is tested. However, in 2006, we finished to build a continuous lab pilot for thermal treatment (pyrolysis,

Table 8 – Composition of inlet hot gas flowrate.

Product	Composition [%v]
Nitrogen	60
Oxygene	2
Water	12
Carbone dioxyde	26

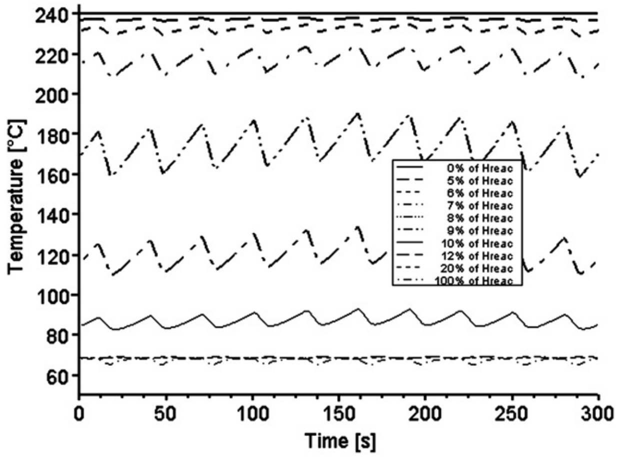

Fig. 8 – Gas temperature evolution over the time at different positions of the reactor.

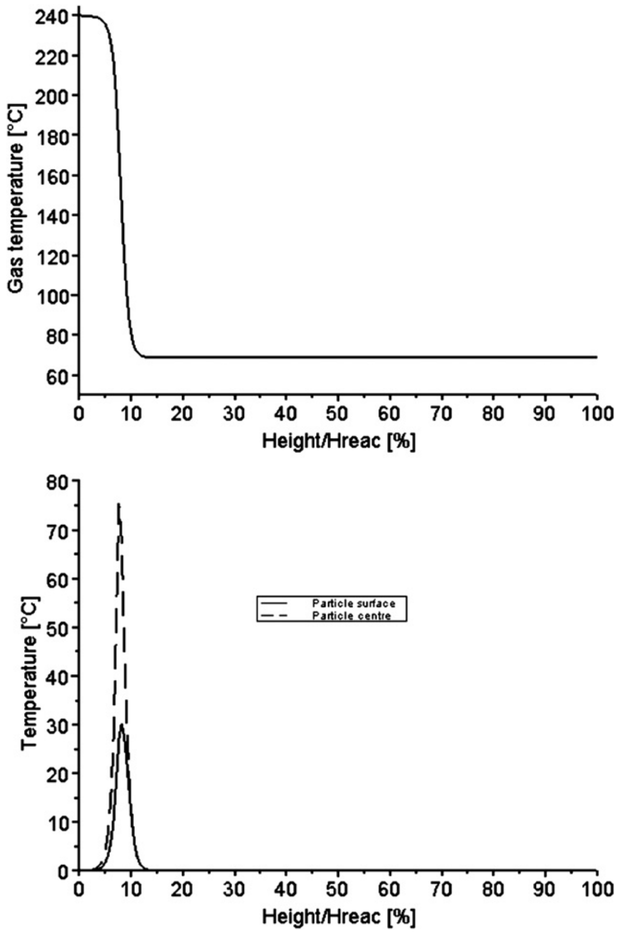

Fig. 9 – Averaged gas temperature evolution over the axial coordinate; temperature differences between gas and surface and centre particles.

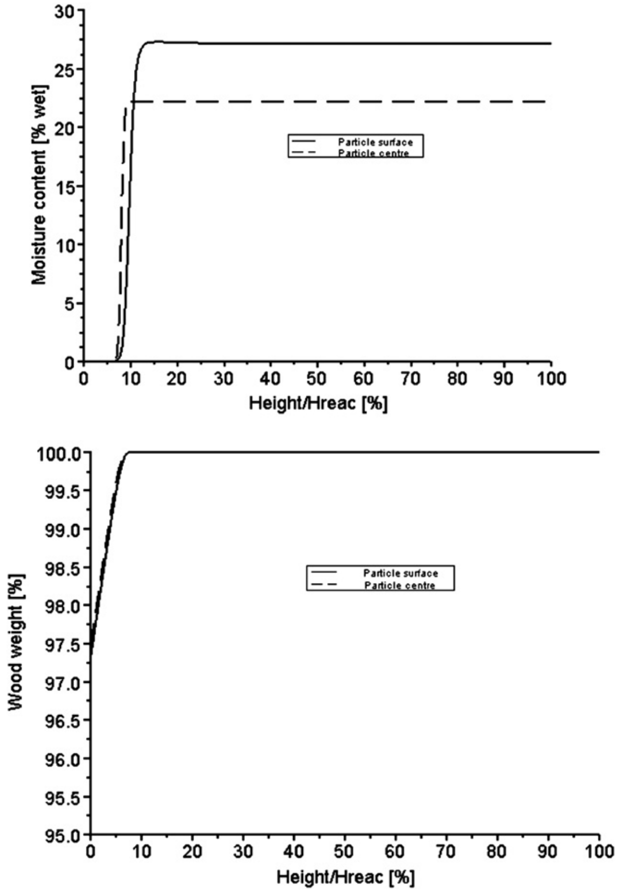

Fig. 10 – Moisture content evolution and wood composition over the axial coordinate.

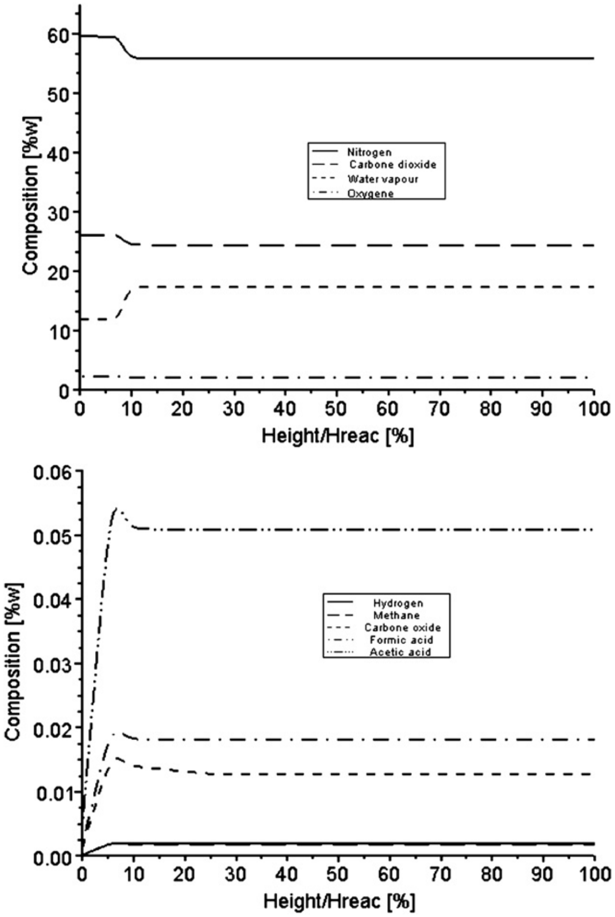

Fig. 11 – Gas composition evolution over the axial coordinate.

torrefaction, gasification) of biomass (maritime pine, olive cake, corn straw). This pilot able to produce 3 kg/h of torrefied biomass is fully instrumented and automated. So, before looking at simulations and results of an industrial TORSPYD reactor, it is interesting to compare experimental data to those obtained with the numerical model. However, firstly it is important to describe the pilot plant and operational procedures used as it proceeds on torrefaction process.

3.1. *Experimental validation*

3.1.1. *Description of the continuous pilot reactor*

The operating reactor uses using a mix of nitrogen and air as a gas source (Fig. 6). The content of oxygen in the inlet gas flowrate is controlled by an oxygen sensor and can be modified by regulating valve A and valve B. One electric coil provides the heat required to reach the necessary temperature of the gas. Once heated up, the inert hot gas is injected at the bottom of the reactor which is a vertical cylinder. Its temperature and its quantity are measured. It is also possible to inject liquid water into the column to provide a vapour water source.

Fresh biomass is fed through a hopper situated at the top of the reactor. Outlet gas is cooled and cleaned in three sequenced baths (Fig. 6).

The entire reactor equipped with several captors, is completely automated and is linked to a computer on which Labview is installed, software dedicated to graphical programming for measurement and automation.

Table 9 – Results from different simulations for several moisture content value.

	Production of 2.8 t/h of torrefied wood						
Moisture of entering particles [% w. basis]	0	5	10	15	20	40	50
Gas flowrate [kg/h]	7000	9000	10900	12100	15000	30000	38000
Gas flowrate/Production	2.5	3.21	3.89	4.32	5.36	10.7	13.6
Power injected [kW]	426	528	664	736	913	1826	2313
Injected power/Production [kWh/kg of torrefied wood]	0.152	0.195	0.237	0.263	0.326	0.652	0.826

3.1.2. Simulation and experimental results

In order to validate the model presented previously, experiments were carried out on the continuous pilot reactor for the production of torrefied wood. Experimental production is calculated by measuring the mass of torrefied wood produced and the mass of the fresh that remains in the hopper. The production is equal to 0.9 kg/h. Inlet particles contains 10% of humidity and are assimilated to spheres of 0.025 cm radius. The porosity bed was measured to be equal to 0.52. Nitrogene and air are injected at a flowrate of 5 Nm^3/h (1 %mol of O_2). At the bottom of the reactor, 135 mL/h of liquid water is sent. By using all those data, it is possible to perform a simulation and compare the different temperature profiles inside the column.

Evolutions of the gas temperature inside the reactor from experimental measured temperatures and from simulated temperature have been plotted (Fig. 7). Although a maximum difference of 18 °C can be observed between the two curves, the evolution tendency of those two curves is quite well represented.

3.2. Industrial TORSPYD reactor simulations for 2.8 t/h of torrefied wood

The geometry of reactor and its dimensions determine the residence time of the solid particles inside the column. This last has got a cylindrical form with a bed height H_{reac} and internal diameter D_{reac}. For confidential reasons, all following results will be adimensionless represented.

Inlet solid particles are considered to have a spherical geometry of a radius $R_{part} = 0.5$ cm and fed into the reactor at 20% moisture content (wet basis). The desired production is equal to 2.8 t/h of torrefied wood which permits to calculate $U_{part}(t)$.

3.2.1. Initial conditions and start up

Before the start-up of the reactor, the column contains particles at 20% moisture content and the bed porosity is fixed to $\epsilon_{reac} = 0.62$ (measured by in our laboratory). The temperature inside the reactor, for both gas and particles, is equal to 20 °C. Then, hot gas is injected at 240 °C at the bottom of the column. The volumetric composition of the gas is known (Table 8).

Feeding and extraction are activated as soon as the temperature closed to the grid reaches 240 °C and as the wood layer at the bottom of the column is torrefied. Extraction is made every 60 s during 15 s at fixed velocity of instantaneous extraction.

3.2.2. Steady state results

At steady state, where the temperature closed to the grid is unaffected by extraction of the solid and keeps its value to 240 °C, the mass gas flowrate that is necessary is equal to 15,000 kg/h to produce 2.8 t/h of torrefied wood from a fresh wood particle with 20% of moisture content. Fig. 8 represents the evolution of gas temperature over time, during five periods of extraction and for different axial positions of the reactor.

The temperatures at the bottom and the top are unaffected by extraction steps of torrefied wood and by feeding steps of fresh particles (Fig. 8). However, a significant transient evolution of the profile of temperature can be observed up to 6% height of H_{reac}. At 8% height, a variation of 20 °C is observed each 35 s, time between the end of one extraction step until the beginning of the next one. Beyond, this temperature variation tends towards to become weaker. This variation is nul up to 20% height of H_{reac}.

If the gas temperature inside the column is time averaged (Fig. 9), one can conclude that only less than 10% of the reactor is

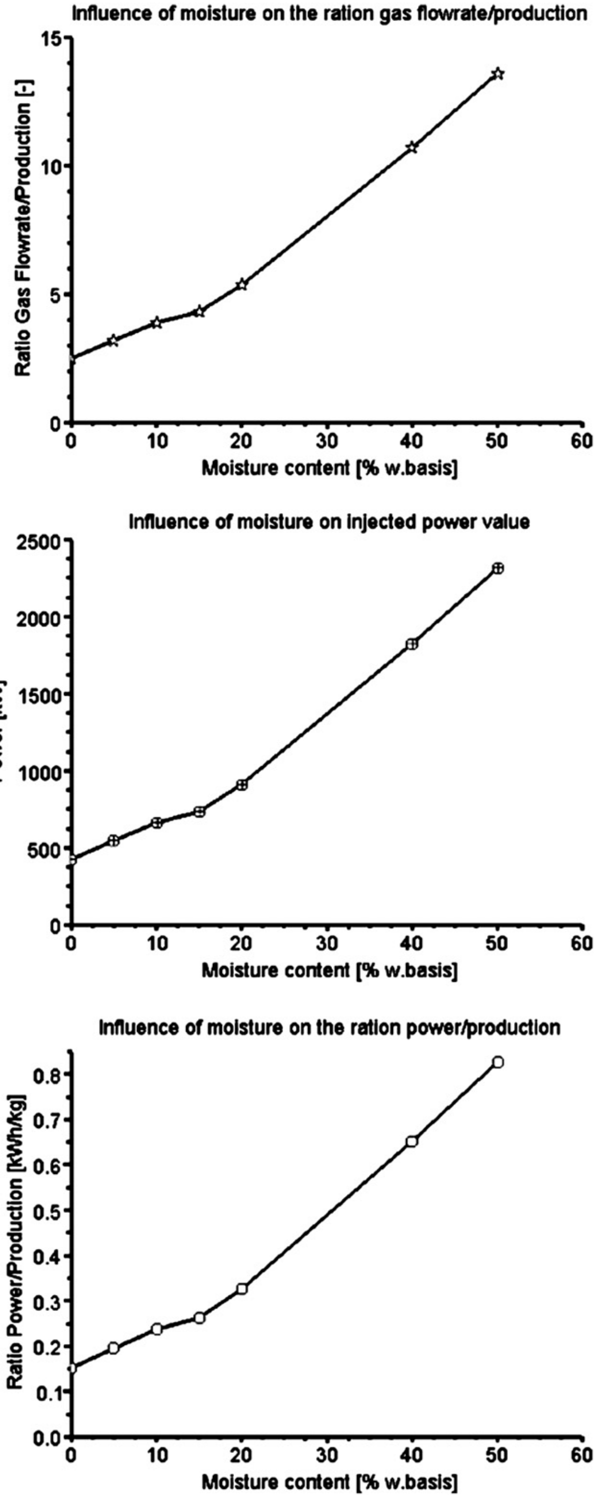

Fig. 12 – Ration Gas flowrate/Production, Power and Ration Power/Production versus Moisture content.

where the thermal degradation occurs. The remainder of the reactor is dedicated to the drying step of the particle and to acting as a filter (condensation) for water and tars. One can say that 15% and 100% of *H*reac can be ignored in the process as Fig. 9 shows no evolution of gas temperature and particle temperatures.

However, as entering the reactor at 20% moisture content, fresh particles firstly absorb water coming from lower wood layers, water vapour coming from drying and from inlet gas flowrate. Water vapour condensates on the surface of the particles and transfers through the pores to the centre of the solids. Moisture content at the surface reaches the value of 27.5% of moisture whereas at the centre of the solids, this value is equal to 22.5% (Fig. 10). There is equilibrium between heat transfer and required energy due to the drying step. Particles act as a filter for the water vapour but also for tars coming from torrefaction reactions. Water flux is going from the gas to the solids.

However, when this equilibrium turns over, gas temperature grows up and water gas saturation increases consequently. It provokes a drying step that first operates at the surface of the particles. Desorption and evaporation of water make temperature of the particle decrease and thermal disequilibrium takes place between the gas and the particles. This disequilibrium tends to go down and to be zero as soon as the drying step is finished. Then, heat transfer leads to an equalization of temperature between the gas and the particles (Fig. 9).

From this precise point where thermal level is sufficient, reactions of torrefaction start. These last get organized between a height of between 0% and 7% of the height of the reactor (Fig. 9). The temperature starts therefore to augment to 240 °C at the bottom of column (Fig. 9). This increase of temperature drives mass wood concentration to reduce in a homogeneous way (Fig. 10). It leads to a final loss of mass (on dry basis) of about 3% at the extraction of torrefied particles.

These reactions also drive to a modification gas composition as tars and light gases are formed. Gases going out of the reactor are predominantly composed of nitrogen (Fig. 11). However, an important content condensable is evident. This level of condensable is due to water present in the inlet gas. This last comes from feeding in hot gases but also from stage of thermal deterioration and in most cases from stage of drying. The tars such as formic acid and acetic acid phenol are in weak in term of their concentration.

Under those conditions of flowrate (gas and particle), the process is able to produce 2.8 t/h of torrefied wood from 20% moisture wood. However, moisture content of freshly cut down woods is usually up to 40%. Consequently, it seems important to study the influence of the moisture value of entering particles.

3.2.3. *Influence of the moisture content and energy of torrefaction*

Previously, it was seen that 15,000 kg/h of gases (composition is given by Table 8) at 240 °C are necessary to produce 2.8 t/h of torrefied wood from fresh wood particles of 20% moisture content. At given composition, flowrate and temperature of the gas, it corresponds to amount of energy injected in the system. The following Table 9 was elaborated by changing the input value of the moisture content in the numerical program. Several simulations were launched considering moisture content going to 0%–50%. In parallel, results presented in Table 9 permitted to plot a set of curves (Fig. 12).

From those curves (Fig. 12), it is possible to say that the variation of the moisture content of the fresh wood particle on torrefaction process and TORSPYD has a linear influence.

4. Conclusions

The work presented in this study is devoted to the mathematical modelling of biomass particle torrefaction in reactor in counter-flow. The first application of the model is the design of the reactor of TORSPYD process. Since 2006, our company has been carried out experiments on the torrefaction process for different type of biomasses with a continuous pilot plant. The model, able to compute several profiles (temperatures, compositions) inside TORSPYD reactor, was first compared with experimental temperature results. It has proved the good ability of the model in predicting accurate gas temperature profiles.

By modelling a 2.8 t/h production reactor, numerical predictions showed the thermal degradation get organized according between an altitude of between 0% and 7% of the height of the reactor whereas the rest of the reactor is dedicated to the drying and the “filter” steps.

At last, the model has permitted the study the influence of the moisture content of the fresh particles to treat. Operational parameters such as the energy flowrate at the bottom of the column and moisture content are crucial on efficient functioning of the reactor TORSPYD.

However, as the pilot reactor is equipped with three gas dryer condenser, analysis of the composition of the gas leaving out the reactor will have to be done in order to compare it with the numerical predictions. It will be investigate soon by our laboratory.

Acknowledgements

The authors like to thank ABAC-CFH for having grinded a 10 kg torrefied wood probe. ABAC-CFH brought its experiences about biomass and coal grinding and combustion.

They like to thank Loïc Guitton for carrying out the torrefaction experiments on the continuous pilot plant.

Nomenclature

A_i	Arrhenius pre-exponential factor of the chemical reaction (s^{-1})
C_p	Heat capacity (J/kg.K)
D^i_{eff}	Effective diffusity of gaseous species i (m^2/s)
D^{int}_{reac}	Internal diameter of the reactor (m)
E_i	Activation energy of the chemical reaction i (J/mol)
h	Enthalpy (J/kg)
H_{global}	Global heat exchange coefficient ($W/m^2/K$)
$h_m(i)$	Mass transfer coefficient for species i (m/s)
*H*reac	Height of the reactor (m)
h_T	Heat transfer coefficient ($W/m^2/K$)
k_i	Kinetic constant of the chemical reaction i (s^{-1})
M	Total moisture content
M_{gas}	Molecular weight of the gas (kg/mol)

n_{part}	Number of particles per reactor volume unit
Nu	Nusselt number
P	Pressure (Pa)
R_g	Perfect gas constant (8314 J/mol.K)
R_{part}	Particule radius (m)
R_i	Rate of production of the species i (kg/m^3.s)
Re	Reynolds number
Pr	Prandtl number
SC	Schmidt number
Sh	Sherwood number
S	Surface (m^2)
t	Time (s)
T	Temperature (K)
U	Velocity (m/s)

Subscripts

b	Bound water
c	Char phase
g, gas	Gas phase
l	Free or liquid water phase
w,W	Dried wood phase

Superscripts

b	Bound water
c	Char phase
g	gas Gas phase
l	Free or liquid water phase
part	Relative to the particle
react	Relative to the reactor
w,W	Dried wood phase

Greek letters

ϵ	Porosity
ϵ_α	Volumique fraction α phase
λ	Thermal conductivity (W/m.K)
μ	Dynamic viscosity (Pa s)
ρ	Density of α phase (kg/m^3)

REFERENCES

[1] Repellin V, Govin A, Rolland M, Guyonnet R. Energy requirement for fine grinding of torrefied wood. Biomass Bioenergy 2010;34:1–8.

[2] Bergman PCA. Combined torrefaction and pelletisation; 2005.

[3] Bridgeman T, Jones J, Shield I, Williams P. Torrefaction of reed canary grass, wheat straw and willow to enhance solid fuel qualities and combustion properties. Fuel 2008;87: 844–56.

[4] Prins M, Ptasinski K, Janssen F. Torrefaction of wood part 1. weight loss kinetics. J Anal Appl Pyrolysis 2006;77:28–34.

[5] Yang H, Yan R, Chen H, Ho Lee D, Zheng C. Characteristics of hemicellulose, cellulose and lignin pyrolysis. Fuel 2007;86: 1781–8.

[6] Beekes ML, Kleinschmidt CP, Meijer R. Torrefaction to improve the sustainability of a coal fired powerplant. Katowice: COAL-GEN; 2009.

[7] Leboutte D. Industrial wood roasting intellectual Property, technologies; 2009. Piracicaba.

[8] Fonseca Felfli F, Alberto Luengo C, Beation Soler P, Rocha Dilcio J. Mathematical modelling of wood and briquettes torrefaction. Procedings of the 5th encontro de energia no meio rural; 2004.

[9] Shafizadeh F, Chin P. Thermal deterioration of wood. Wood technology: chemical aspects. In: ACS Symp. Ser, Vol. 43; 1977. 57–81.

[10] Ratte J, Marias F, Vaxelaire J, Bernada P. Mathematical modelling of slow pyrolysis of a particle of treated wood waste. J Hazard Mater 2009;170:1023–40.

[11] Whitaker S. Simultaneous heat, mass, and momentum transfer in porous media: a theory of drying. Adv Heat Transf 1977;13:119–203.

[12] Casajus C. Torréfaction de biomasses ligno-cellulosiques. Université de Pau et des Pays de l'Adour; 2010.

[13] Thurner F, Mann U. Kinetic investigation of wood pyrolysis. Ind Eng Chem Proc Des Dev 1993;19:71–104.

[14] Reppelin V. Optimisation des paramètres durée et température d'un traitement thermique du bois: modifications des propriétés d'usage du bois en relation avec les modifications physico-chimiques et ultrastructurales occasionnées par le traitement thermique. Ecole Nationale Supérieure des Mines de Saint Etienne; 2006.

[15] Dryer F, Glassman I. High temperature oxidation of co and ch4. Proceedings of the 14th Symposium (Int.) on combustion, Pittburgh 1973;987–1003.

[16] Kerinin E, Shifrin E. Mathematical model of coal combustion and gasification in a passage of an underground gas generator, combustion, explosion and shock waves. Russia: Academy of Sciences; 1993. 148–154.

[17] Biba V, Macak J, Klose E, Malecha J. Mathematical model for the gasification of coal under pressure. Ind Eng Chem Proc Des Dev 1978;17:92–8.

[18] Chang J, Chen H, Xu S, Lin M. Computational study on the kinetics and mechanisms for the unimolecular decomposition of formic and oxalic acids. J Phys Chem A 2007;111:6789–97.

[19] Blake P, Jackson G. The thermal decomposition of acetic acid. J Chem Soc B; 1968:1153–5.

[20] Bird R, Steward E, Lightfoot EN. Transport phenomena. 2nd ed. New York: John Wiley and Sons, Inc; 2002.